AD-A139 300 MICROSCOPIC STUDY OF THE INFLUENCE OF IMPURITIES ON INTERFACE BONDING(U) TEXAS UNIV AT AUSTIN CENTER FOR MATERIALS SCIENCE AND ENGINEERING H L MARCUS 25 JAN 84 1/1

UNCLASSIFIED UTCMSE-84-1 N00014-83-K-0143 F/G 11/4 NL

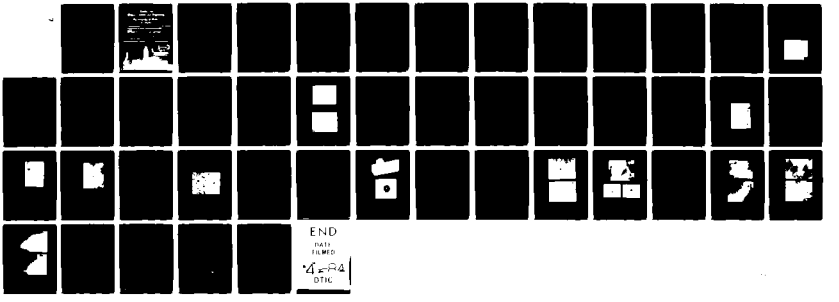

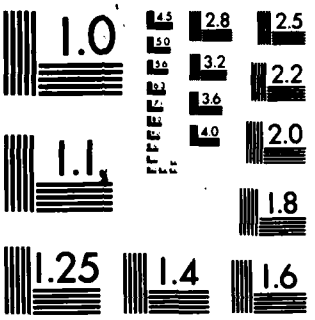

SECURITY CLASSIFICATION OF THIS PAGE (When Data Entered)

REPORT DOCUMENTATION PAGE		READ INSTRUCTIONS BEFORE COMPLETING FORM
1. REPORT NUMBER UTCMSE-84-1	2. GOVT ACCESSION NO. AD-A139300	3. RECIPIENT'S CATALOG NUMBER
4. TITLE (and Subtitle) Microscopic Study of the Influence of Impurities on Interface Bonding		5. TYPE OF REPORT & PERIOD COVERED Annual Technical Report Dec. 1, 1982 - Nov. 30,1983 6. PERFORMING ORG. REPORT NUMBER
7. AUTHOR(s) H.L. Marcus		8. CONTRACT OR GRANT NUMBER(s) N00014-83-K-0143
9. PERFORMING ORGANIZATION NAME AND ADDRESS The University of Texas Mechanical Engineering/Materials Science ETC 5.160, Austin, TX 78712		10. PROGRAM ELEMENT, PROJECT, TASK AREA & WORK UNIT NUMBERS
11. CONTROLLING OFFICE NAME AND ADDRESS Office of Naval Research Metallurgy and Ceramics Program Arlington, VA 22217		12. REPORT DATE January 25, 1984 13. NUMBER OF PAGES 41
14. MONITORING AGENCY NAME & ADDRESS(if different from Controlling Office) Dr. B.A. MacDonald, Metallurgy Division Office of Naval Research, Code 471 Department of the Navy Arlington, VA 22217		15. SECURITY CLASS. (of this report) UNCLASSIFIED 15a. DECLASSIFICATION/DOWNGRADING SCHEDULE
16. DISTRIBUTION STATEMENT (of this Report) Approved for public release; Distribution unlimited.		
17. DISTRIBUTION STATEMENT (of the abstract entered in Block 20, if different from Report)		
18. SUPPLEMENTARY NOTES		
19. KEY WORDS (Continue on reverse side if necessary and identify by block number) Auger Electron Spectroscopy, Interface Characteristics, Interface Fracture, Scanning Auger Microscopy, I/V Switching, Aluminum/Silicon Carbide Discontinuous Fibers, Metal Matrix Composites, Aluminum/Graphite Composites		

20. ABSTRACT (Continue on reverse side if necessary and identify by block number)

Results are reported for two experimental areas associated with interface failure. Model layered systems, with the main emphasis on the Al-Al_2O_3-Graphite system, were studied for varied interface chemistry and thickness. The results show that when the interface has low resistivity fracture occurs within the graphite but when the interface resistance is high fracture occurs within the interface. This holds true for a wide range of interface chemistries and impurity doping at the

(Continued)

DD FORM 1 JAN 73 1473 EDITION OF 1 NOV 65 IS OBSOLETE

SECURITY CLASSIFICATION

interface. Introduction of an embrittling element at the interface of the low resistance interface did not change the fracture path.

The second experimental area studied was the influence the interface plays on the fracture behavior of the discontinuous SiC/Al matrix composites. Both discontinuous fibers and particulate SiC dispersoids were studied. In all cases interface failure was not the dominant fracture path. The more ductile the matrix the more ductile the composite and the less interface failure. γ-Al_2O_3 was observed to be present at many of the interfaces.

TABLE OF CONTENTS

Page		
1	I.	Introduction
1	II.	Background
3	III.	Experimental Interface Failure Results of Model Interfaces
6	IV.	Interface Characterization of the SiC/Al Metal Matrix Composites
9	V.	Summary
10	VI.	References
12	Appendix A -	Interface and Fracture Surface Analysis of Discontinuous SiC/Aluminum Metal Matrix Composites
39	Appendix B -	Quantitative Interface Strength Measurement

Microscopic Study of the Influence of Impurities on Interface Bonding

I. Introduction

In this first annual report, two major experimental areas were emphasized. The primary research area was involved in the detailed evaluation of the fracture behavior of specially prepared interfaces and the impact changes in chemistry and electrical characteristics have on that behavior. The second major thrust was the investigation of the interfaces in discontinuous silicon carbide - aluminum metal matrix composites. The early stages of both of these research efforts were reported on earlier (1). A great deal of the results in this report originate in two theses (3,4) as well as more recent studies. Some of the proposed experimental efforts have been delayed due to the Materials Science and Engineering Program at The University of Texas moving into a new facility in a new building. Installation of most of the experimental facilities is now being finished and the new experimental efforts in this research are now finally getting underway.

II. Background

Composite materials have been used in engineering applications for many years (4,5). The development of these materials was based on the concept of using two or more elemental materials brought together to achieve a combination of properties not achievable by any of the elemertal materials acting alone. A composite may include particles, flakes, whiskers, or fibers embedded into a matrix which has the desired

properties for a particular application and many possess long term potential in which light weight and high stiffness are required (6,7). In all cases of the composites, as well as in other structural materials, the interface chemistry and bonding of interfaces, phase boundaries and grain boundaries play a major role in the fracture behavior.

An example is the interface role in the bonding characteristics of the Al/Gr layered system. The interface strength of this system has been observed to be dependent on the thickness of the aluminum oxide layer (8). When the oxide films are thin, the interface is more adhesive and strongly bonded to the graphite. As the oxide thickness is increased the bond between the oxide and the graphite is weakened, as indicated by a change in fracture path.

Another important characteristic of this particular interface structure is its threshold switching behavior. Threshold switching can be described as an abrupt change in resistivity of the structure when it is subjected to sufficiently high electric fields (9). When the voltage is increased above a certain threshold voltage, the resistivity abruptly decreases and will remain in the low resistivity state for some relaxation time.

The purpose of this research is to study the interrelationship between the threshold switching characteristics and the mechanical strength of the interfaces. Systems can be constructed through vapor deposition of thin layers to build the appropriate model interface region. By introducing a thin layered model the investigation of the correlation between electronic and mechanical properties of the system is greatly simplified. This structure allows the easy application

of voltage across the interface which produces the threshold switching to a higher conductivity state and also makes it convenient for testing the mechanical strength of the interface. This is done through peel tests. In the peel test, a force perpendicular to the interface is applied, peeling away the layers with higher cohesive strength exposing the location of the weakest interface. The determination of the composition of the exposed surface is made with the aid of surface sensitive Auger electron spectroscopy (AES). This type of analysis has revealed that when a high conductivity interface state exists the interface between γ-Al_2O_3 and the graphite crystal is more adhesive than when a low conductivity interface state exists.

The proposed origins and bases of the switching phenomenon has been discussed earlier (1) and extensively in the literature (10-14) and will not be repeated here.

III. Experimental Interface Failure Results of Model Interfaces

Peel tests were conducted on a wide range of samples with different switching history. The majority of the effort involved the aluminum/oxide/graphite layered structure. Peel tests were done with samples in four resistivity states. The first is in an intrinsic low resistivity state. The second is in the intrinsic high resistivity state. The third is after switching from the high resistivity state to the low resistivity state by applying a voltage above the threshold voltage. The fourth is in the high resistivity state following relaxation from the induced low resistivity state back to the high resistivity state. Results of some of these measurements were reported previously. During the present research period, the prior work was reproduced extensively and extended into modified interface chemistry.

The interface modifications studied included the following. (1) The use of aluminum alloy deposition instead of pure aluminum. The alloy used was 6061, a favorite in the composite systems. (2) Modifications of the oxide thickness to reduce the applied voltage for switching. (3) Addition of an embrittling element, sulfur, into the interface to see its impact on the fracture behavior. (4) The modification of the oxide resistivity by controlling the deposition parameters.

A schematic of the layered structures is shown in Fig. 1. Fig. 2 shows the characteristic I/V curves of the low and high resistivity states. In the extensive number of tests done to date under all the described conditions the following has been repeatedly observed. (1) When the system is in the high resistivity state the fracture path progresses through the interface region, Path A-Fig. 1. We conclude that when the layered structure is in the high resistivity state the interface is the weak link. (2) When the samples are fractured while in the low resistivity state fracture occurred in the graphite substrate (Path B - Fig. 1). This continued result supports the result that the interface is more adhesive when the interface is conductive. Samples which were switched to the low resistivity state but which were allowed to relax back to the high resistivity state, after removal of the applied voltage, exhibited a fracture surface composition associated with the interface; similar to the fracture path observed in the unswitched samples. This reversibility of the phenomenon has been shown repeatedly.

When the interface oxide was made from vapor deposition of the Al alloy 6061 the interface state was found to have low resistance and the fracture path was through the graphite. Similarly thin oxide

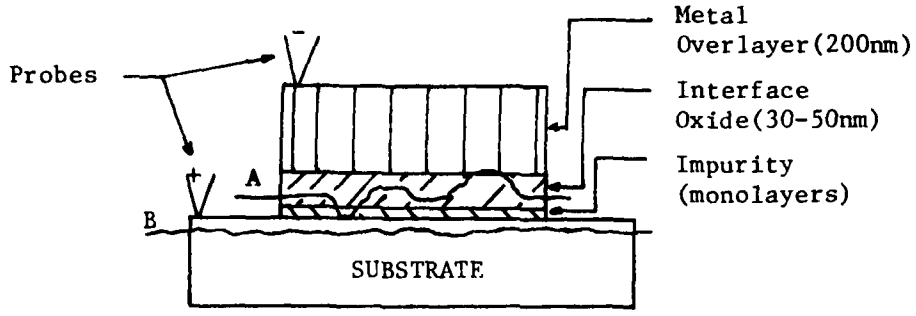

Figure 1: A schematic of the composite layered structure
Path A represents the fracture path in the high resistivity state.
Path B represents the fracture path in the low resistivity state.

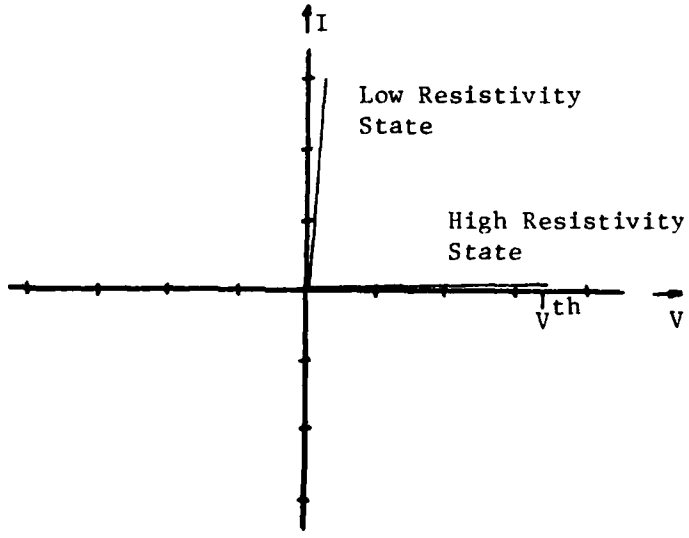

Figure 2: A schematic representation of current-voltage characteristics of the composite layered structure

thicknesses showed easy or no switching and fracture through the graphite. An AES spectra of the fracture in the graphite is shown in Fig. 3. When the oxide was thin and various amounts of sulfur were introduced at the interface the resistivity was low and fracture still occurred in the substrate. The sulfur at the interface is shown by the inert ion sputtering profile through the total layered structure, Fig. 4. The diffuse layer is due to the geometric sputtering effect. The lack of fracture being induced into the interface region by the presence of an embrittling element like sulfur was somewhat surprising. One possible reason could be the lack of wetting by the sulfur as shown for thick sulfur deposits on aluminum in Fig. 5 which has also been observed for S on graphite. A limited number of experimental conditions have been studied to date and additional experiments are presently underway to further investigate the impurity effects.

To make the above results more meaningful the fracture load (stress) must be obtained. Several of the experimental approaches to quantify the measurement currently being tested are described in Appendix B.

IV. Interface Characterization of the SiC/Al Metal Matrix Composites

The objective of this effort was to attempt to identify how the interface in the SiC/Al MMC influenced the fracture behavior. The details of the results are given in Appendix A. What follows is an outline of the experimental approaches used and the significant results. Testing was done on both the discontinuous SiC and the particulate SiC composite materials. The experimental approaches used were mechanical tests, AES of the fracture surface combined with inert ion sputtering,

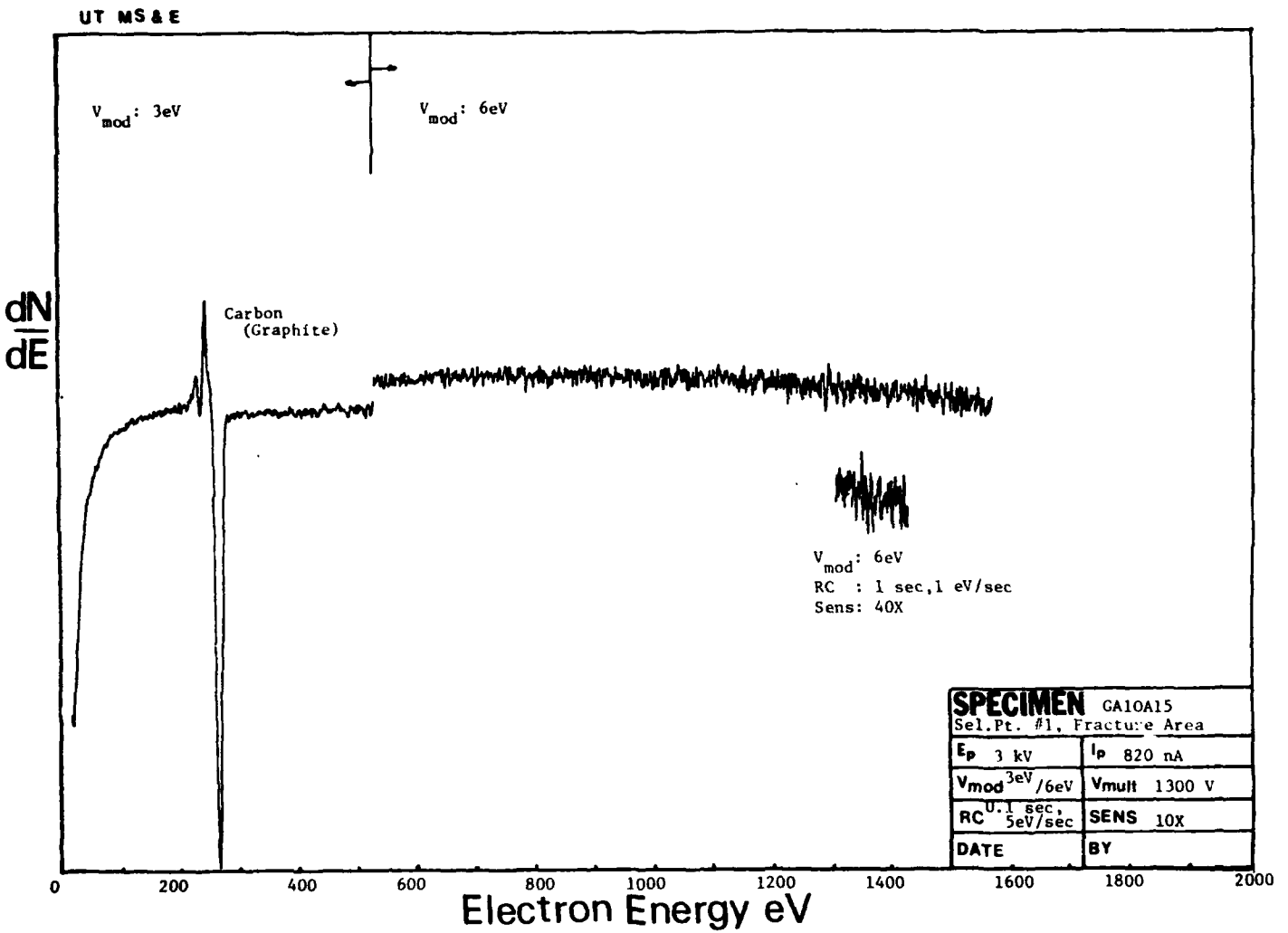

Figure 3: An Auger spectrum of the fracture surface of a Graphite/Aluminum Oxide/Aluminum thin layered structure fractured in the [illegible]al resistivity state.

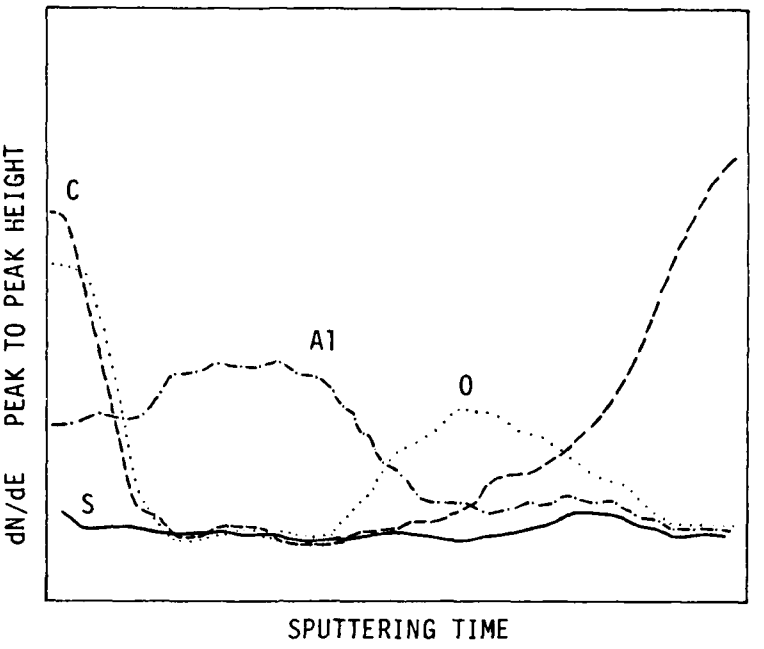

Figure 4. Schematic of AES depth sputter profile of C, O, Al and S from a specimen with sulfur, Al oxide and Al deposited on a graphite substrate.

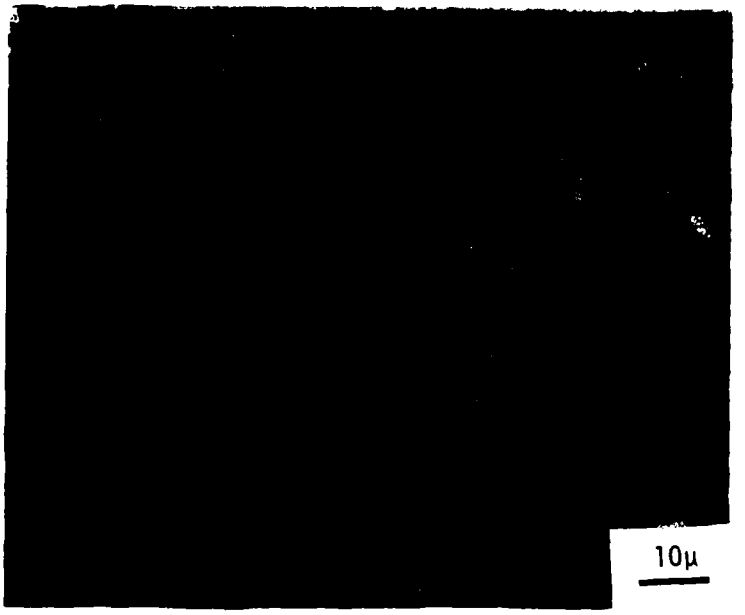

Figure 5. Islands of sulfur on an aluminum vapor deposited substrate.

and TEM of ion thinned specimens. The results show that γ-Al_2O_3 is present at many of the SiC/Al interfaces. The fracture path is not dominated by the interfacial failure but is primarily a matrix failure path. The more ductile the matrix, the less amount of interfacial fracture occurs. The large volume fraction of SiC plays a major role in the fracture behavior by influencing the volume of material being deformed. Some of the deformation energy could have been reduced due to prior formation of dislocation networks due to thermal coefficient of expansion mismatch between the SiC and the aluminum. This was not as apparent in the particulate SiC/Al MMC.

V. Summary

Results are reported for two experimental areas associated with interface failure. Model layered systems, with the main emphasis on the Al-Al_2O_3-Graphite system, were studied for varied interface chemistry and thickness. The results show that when the interface has low resistivity fracture occurs within the graphite but when the interface resistance is high fracture occurs within the interface. This holds true for a wide range of interface chemistries and impurity doping at the interface. Introduction of an embrittling element at the interface of the low resistance interface did not change the fracture path.

The second experimental area studied was the influence the interface plays on the fracture behavior of the discontinuous SiC/Al matrix composites. Both discontinuous fibers and particulate SiC dispersoids were studied. In all cases interface failure was not the dominant fracture path. The more ductile the matrix the more ductile the composite and

the less interface failure. γ-Al_2O_3 was observed to be present at many of the interfaces.

VI. References

1. Harris L. Marcus, Final Technical Report UTMSE-83-1, "Interface Character of Aluminum-Graphite Metal Matrix Composites," January 1983 ONR Contract N00014-78-C-0094.
2. Horacio J. Mendez, M.S. Thesis, The University of Texas at Austin, "Correlation between Threshold Switching and Interface Adhesion in Aluminum-Aluminum Oxide-Graphite Layered Structures," May 1983.
3. Li-Jiuan Fu, M.S. Thesis, The University of Texas at Austin, "The Interfacial Characterization of Discontinuous Silicon-Carbide and Continuous Graphite Fiber Reinforced Aluminum Composites," August 1983.
4. A. Kelley, Composites 10 (1979), p. 2.
5. B.R. Noton, ed., Composite Materials, Vol. 3: "Engineering Applications of Composites," Academic Press, New York, 1974.
6. A.A. Watts, "Commercial Opportunities for Advanced Composites," ASTM 704, American Society for Testing Materials, Philadelphia, 1980.
7. M.F. Amateau. Journal of Composite Materials 10 (1976) p. 279.
8. Swe-Den Tsai, Ph.D. dissertation, The University of Texas at Austin 1980.
9. D.F. Weirauch, Appl. Phys. Letters 16 (1970) p. 72.
10. H.J. Stocker, Appl. Phys. Letters 15 (1969) p. 5.

11. G.C. Vezzoli, P.J. Walsh and L.W. Doremus, J. Non-Crystalline Solids 18 (1975), p. 332.

12. H.K. Henisch, E.A. Fagen and S.R. Ovshinsky, J. Non-Crystalline Solids 4 (1970) p. 438.

13. W. Van Roosbroeck, Phys. Rev. Letters 28 (1972) p. 1120.

14. K.E. Petersen and D. Adler, Appl. Phys. Letters 27 (1975) p. 625.

Appendix A

Interface and Fracture Surface Analysis of Discontinuous SiC/Aluminum Metal Matrix Composites

Introduction

In this appendix studies of the fracture surface and the interface between the discontinuous SiC and aluminum matrix are described. The development of these materials is described elsewhere (1-3). The mechanical properties were measured and the fracture surface behavior investigated with Auger electron spectroscopy, AES. The interfaces were observed on ion thinned specimens in the TEM. It should be clearly realized that the materials investigated were representative of the processing development of both the discontinuous fiber SiC/Al composite (ARCO, SILAG) and the particulate SiC/Al composites (D.W.A.) at the time of the study. The materials were not optimized at that time and subsequent improvement in properties has been made by improved processing.

Silicon-Carbide Discontinuous Fibers in Aluminum Alloys

Material Description

The following are the six types of silicon-carbide discontinuous fiber in aluminum matrices composites:

1. A6013Z: SXA 2024 + 22.45 w/o F-9 Grade Silicon Carbide, flat, ½"x5"x1-7/8", as ex[illegible]
2. C0115Z: SXA 6061 [illegible]-9 Grade Silicon Carbide, flat, ¼"x1½"x1-3/4", as [illegible]

3. C0116Z: SXA 6061 + 30 w/o F-9 Grade Silicon Carbide, flat, 1/8"x2-5/16"x1-9/16", as extruded.
4. D0026Z: SXA 7075 + 20 w/o F-9 Grade Silicon Carbide, flat, ¼"x1½"x2", as extruded.
5. D0030Z-2: SXA 7075 + 5.7 w/o F-9 Grade Silicon Carbide, rod, 5/8"x1-3/4", as extruded.
6. E0019Z-2: SXA Al-5% Li + 25 w/o F-9 Grade Silicon Carbide, rod, 5/8"x1-3/4", as extruded.

The particulate SiC/Aluminum composite was 25 v/o silicon-carbide powder blended in Al 6061 metal-matrix. These are dispersion-strengthened composites. In order to evaluate both the silicon-carbide discontinuous fiber reinforced and silicon-carbide powder reinforced aluminum MMC, tensile tests, AES and SEM fracture surface analyses, as well as TEM microstructural analyses were performed.

Experimental Approaches

Specimens of the SiC/Al MMC's were mounted in a mixture of 5 parts of Buchler Epo-Kwick Resin and 1 part of Epo-Kwick Hardener and etched in Keller's reagent [2 ml HF (48%), 3 ml HCl (conc), 5 ml HNO_3 (conc), 190 ml water] for a second, and then observed under an optical microscope. The optical microscope used was the CARL ZEISS metallograph with ultraphoto camera system. Dark areas on the surface, at 2500X, (Fig. A1) were regions of higher silicon-carbide content. In order to observe the silicon carbide fiber at higher magnification, scanning electron microscopy was used. Metallurgical specimens were etched by HCl for a second, then washed by methanol. Figure A2 shows a sample after the chemical etching. The

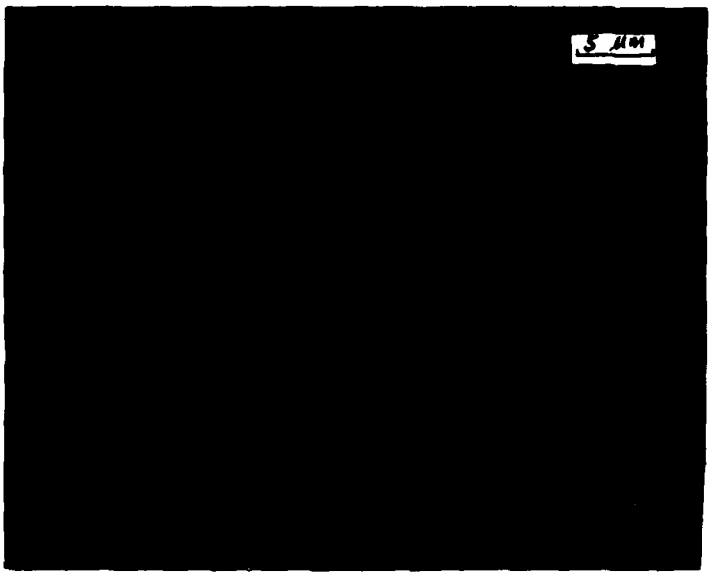

Fig. A1. A typical optical micrograph of the metallurgical Si-carbide discontinuous fiber/Al composite specimen. The dark area shows the Si-carbide region.

Fig. A2. The SEM observation of the above surface etched by HCl. The diameters of the fibers are very small, varying from 0.2 μm to 1 μm.

Al metal matrix was etched away and some fibers were left sticking out of the surface. The diameters of the fibers vary from 0.2 to 1 μm.

Mechanical Testing

Tensile tests of six types of silicon-carbide discontinuous fiber/Al composites and silicon-carbide powder/Al composite were accomplished by using a standard Instron Tensile Tester model 1125. Rectangular specimens were carefully machined from composite plates, rods, or sheet. Four tabs were carefully glued onto each specimen using a high shear strength epoxy glue, Mill-Stephenson type 907 adhesive (4). A crosshead speed of 1 mm/min and 10 KN full scale load were used for testing these composites. The reduced section was 0.5 inches for the discontinuous SiC fiber Al MMC's and 2.0 inches for the particulate SiC/Al MMC's.

AES Analysis of the Fracture Surfaces

Samples from all of the silicon-carbide discontinuous fiber/Al composites and the 25 v/o silicon-carbide powder/Al composite were fractured inside the ultra high vacuum chamber (10^{-9} - 10^{-10} torr) to avoid contamination of the surfaces. The discontinuous fibers or the particle sizes are below the resolution of the Auger spectrometer. Therefore, a square rastered beam of 3 μm and a magnification of 1000X scanning at a TV rate were used to collect the average compositional AES information from the fracture surfaces. The quantitative AES analysis of the compositional ratio of Al to Si in the spectrum was done by measuring the peak to peak heights of Al and Si from a dN(E)/dE curve and correcting by the relative sensitivity factors obtained from the standard Auger handbook (5). The studies were carried out in a Physical Electronics 590 SAM system using a nominal 1 micron beam size.

SEM Investigation

The silicon-carbide discontinuous fiber/Al composites and silicon-carbide powder/Al composite were fractured and quickly put into the SEM vacuum chamber to prevent the fracture surfaces from oxidizing in air. A JEOL JSM-35C model SEM with KEVEX energy dispersive spectroscopy system (EDS) was used for topological and chemical analysis.

Ion Beam Thinning

An Edwards IBT 200 ion beam accessory was used to prepare the TEM specimens. The unit has two guns to bombard both sides of a specimen at the same time. The specimen must be mounted at the right height and be tilted a suitable angle, so that the ion beam can hit the specimen from both sides. Since the specimen is very thin, the larger the tilt angle, the easier it is for the specimen to slip out of the center. Thus, the suitable tilt angles for sputtering are between 10° and 30°. The specimen chamber was evacuated to about 10^{-5} torr, then argon gas was bled into the two guns causing the operating pressure to increase to between 10^{-2} and 10^{-3} torr. In order to get even sputtering, the specimen holder was rotated at a few rpm. Typically, 1-2 μm/hr per side of specimen was removed, so that a 30 μm specimen took 10 to 30 hours to be thinned sufficiently for electron transmission, while a 100 μm specimen took a few days to thin. It is therefore important that the specimen be thinned as far as possible using mechanical means before starting on the ion beam thinning.

The following is the method used in preparing the silicon-carbide/Al and graphite/Al composites specimens for the ion beam thinning. First,

the specimen was sliced to a thickness of about 150 μm from the bulk material by a diamond wheel blade, then one side of the specimen was ground very carefully with 600 grade abrasive paper to get a polished surface. The polished side of the speicmen was then glued to a glass slide with Duco cement. A guard ring made from brass (about the same hardness material as the specimen) of about 200 μm was glued on the glass slide to surround the specimen. The specimen and guard ring were then simultaneously ground down to about 20 to 30 μm by using a flat surface covered with 600 grade abrasive paper. The specimen and guard ring were separated from the glass slide by immersion in acetone for about 10 to 20 minutes. The specimen could then be fitted into the sample holder of the ion beam thinning machine.

TEM Analysis

For the TEM microstructural and interfacial studies, four kinds of materials were prepared by ion beam thinning and for one of them both ion beam thinning and jet polishing was used to get the thin regions (the as-received silicon-carbide fiber/Al composite-A6013Z specimen). The jet polishing solution used was a mixture of 2% hydrochloric acid, 49% nitric acid and 49% methanol. The as-received A6013Z prepared by ion beam thinning technique was sliced in a transverse section*. In an attempt to widen the interface region, the A6013Z specimen was heat treated by encapsulating the specimen at the diffusion-pumped rough vacuum condition (about 2×10^{-4} torr) in a vycor glass tube and heat treated at 550°C for 24 hours. The heat treated specimen was then sliced in both transverse and longitudinal* sections and followed by ion beam thinning.

Both the as-received and after tensile test specimens of silicon-carbide discontinuous fiber/aluminum composite-C0116Z and 25 v/o silicon-carbide powder/aluminum composite were prepared by ion beam thinning technique for TEM microstructural and interfacial studies. The TEM work from the jet polished A6013Z specimen was done using the JEOL JEM-150 while all the other TEM work was performed using the JEOL JEM-200CX.

Results and Discussion

Mechanical Tests

The stress-strain curves showed that silicon-carbide/aluminum composites had substantially ductile fracture. The results of tensile tests of the SiC/Al composites are listed in Table 1, the strength measured was the ultimate tensile strength (U.T.S.). For the same Al alloy matrix, the more SiC fiber reinforcement, the stronger the material, but the lower the ductility. A special case is that of the metal matrix of E0019Z-2. The ductility of the alloy matrix is significantly reduced when the lithium concentration exceeds about two percent (5).

SEM Analyses

SEM fractography showed a ductile-dimple fracture mode on the matrix fracture surfaces of the silicon-carbide discontinuous fiber/Al and silicon-carbide powder/Al composites. It was rare to find fibers on the fracture surfaces of Si-carbide discontinuous fiber/Al composites. A comparison

---

*TEM observations indicated that there was a preferred orientation of the fiber of A6013Z specimen, thus transverse and longitudinal sections could be defined.

Table 1. A comparison of mechanical properties of Si-carbide/Al composites with matrix alloys and Si-carbide contents.

Material	Metal Matrix	SiC	U.T.S. of MMC (ksi)
A6013Z	2024	22.45 w/o	66
C0115Z	6061	10 w/o	43
C0116Z	6061	30 w/o	65
D0026Z	7075	20 w/o	64
D0030Z-2	7075	5.7 w/o	63
E0019Z-2	Al-5% Li	25 w/o	47
SiC powder/Al	6061	25 v/o	33

of the fracture surfaces of D0026Z (Al 7075 + 20 w/o Si - carbide fiber), A6013Z (Al 2024 + 22.45 w/o Si-carbide fiber) and E0019Z-2 (Al-5% Li + 25 w/o Si-carbide fiber) follows. Al 7075 is a more ductile matrix alloy than the Al 2024 and Al-5% Li alloys. The three composites have about the same fiber content by weight. The SEM micrograph in Figs. A3, A4 and A5 illustrate the limited number of fibers on the D0026Z fracture surface, but the more predominant presence of fibers on the E0019Z-2 and A6013Z fracture surfaces. This was consistent with the results of AES quantitative analysis that follow.

It was very difficult to distinguish between the Al matrix and Si-carbide powder particles at the fracture surface of Si-carbide powder/Al composite. As a result of SEM silicon-mapping, as shown in Fig. A6, it is evident that the size of the Si-carbide particles varies with some as large as 10 μm. The spacing between the particles was not uniform.

AES Results

Auger electron spectra collected from the fracture surfaces of the Si-carbide discontinuous fiber/Al alloy composites showed very small Si peaks compared to the theoretical ratio of Si to Al for the weight fraction of Si-carbide present. An extreme case is that of D0030Z-2, the ratio of Al to Si is 88 to 1 which means that there is effectively no Si at the fracture surface. After extensive inert ion sputtering (removal about 0.5-1 μm) of the surfaces, increased silicon-carbide was observed on most of the fracture surfaces. Figures A3, A4 and A5 show the AES spectra of fracture surfaces of the specimens before and after sputtering along with the SEM fracture surface pictures. The results

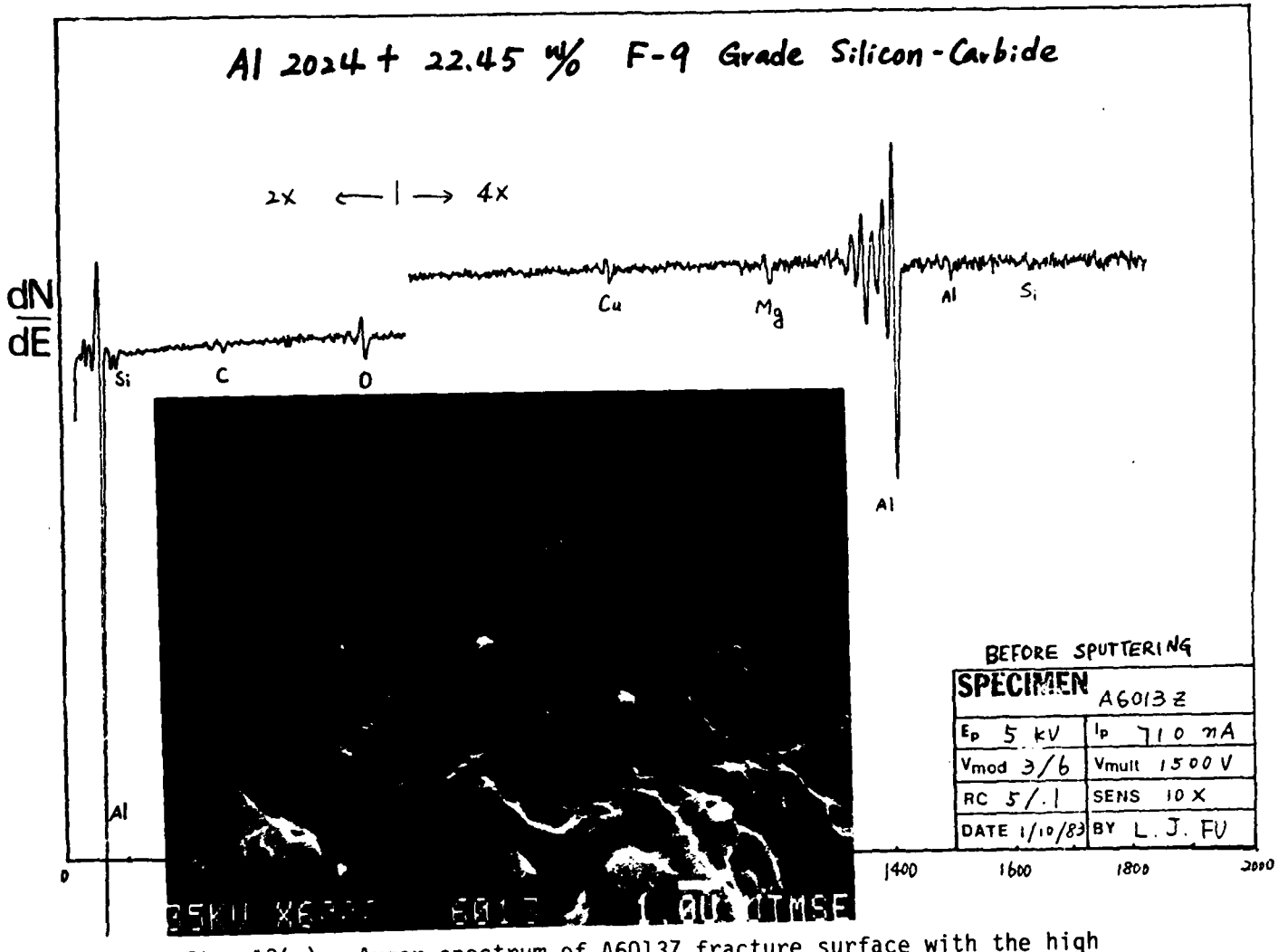

Fig. A3(a). Auger spectrum of A6013Z fracture surface with the high magnification SEM micrograph of the specimen.

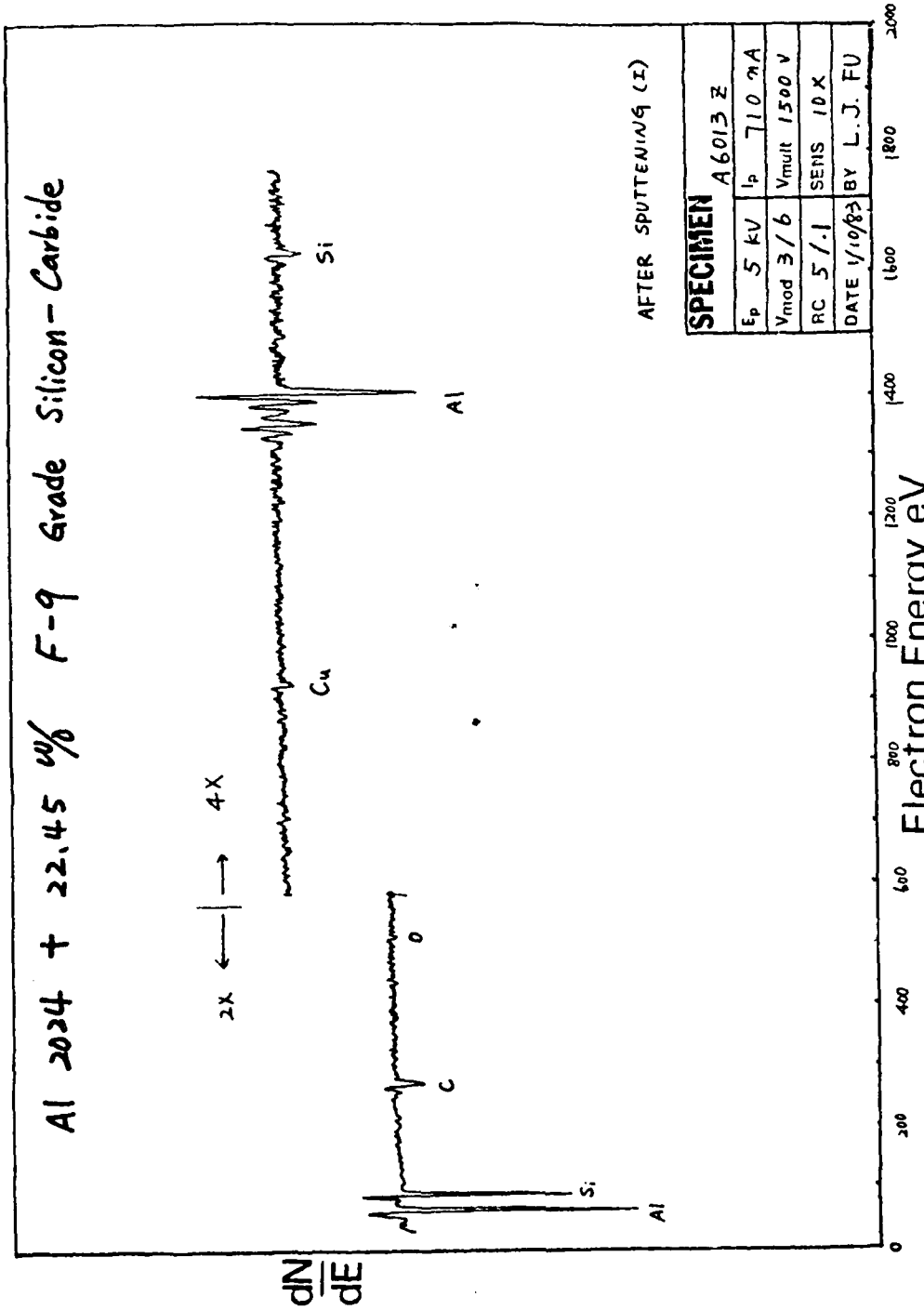

Fig. A3(b). AES of fracture surface of A6013z after inert ion sputtering (removed about 0.5 μm) shows more SiC on the surface.

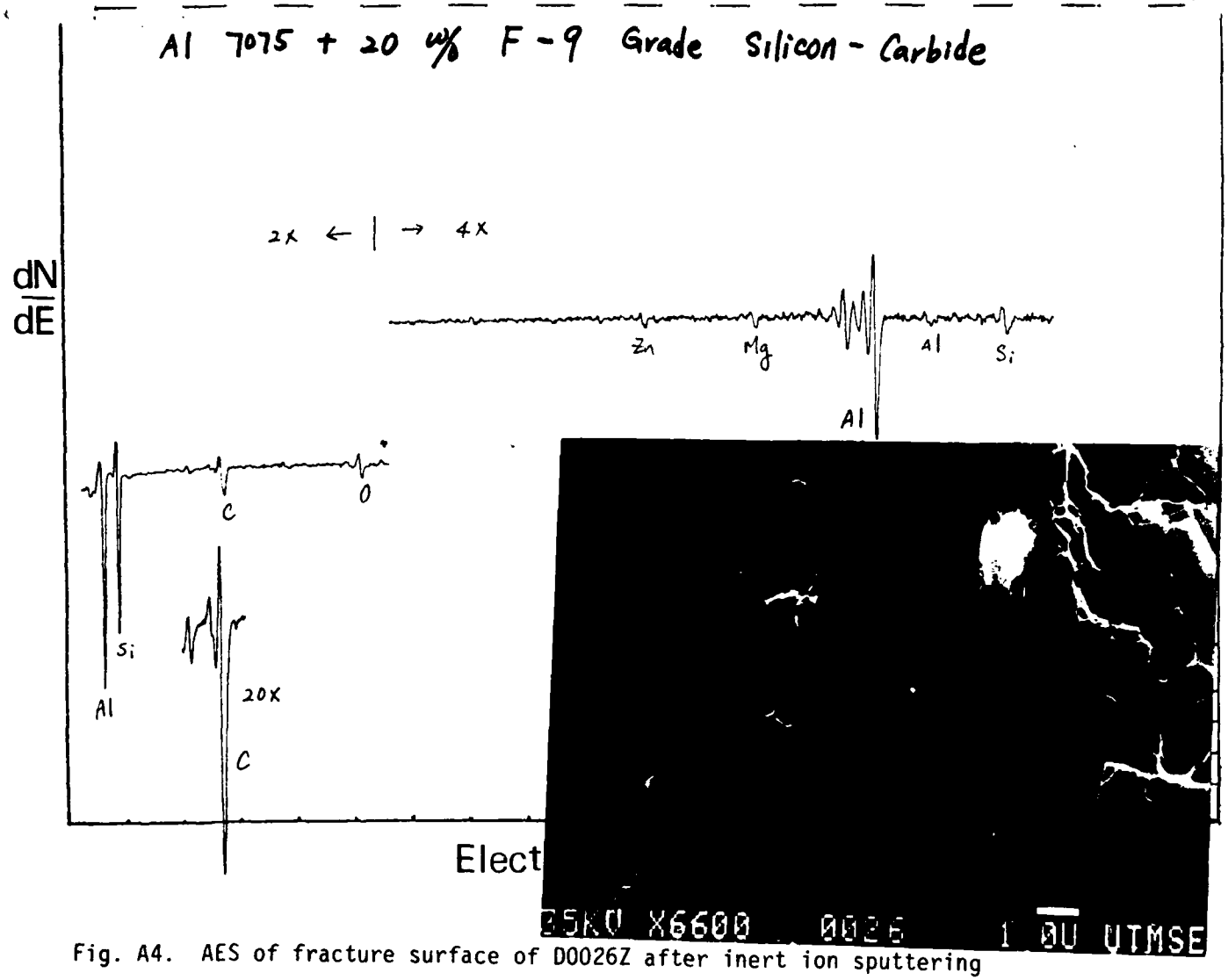

Fig. A4. AES of fracture surface of D0026Z after inert ion sputtering (removed about 0.5 μm).

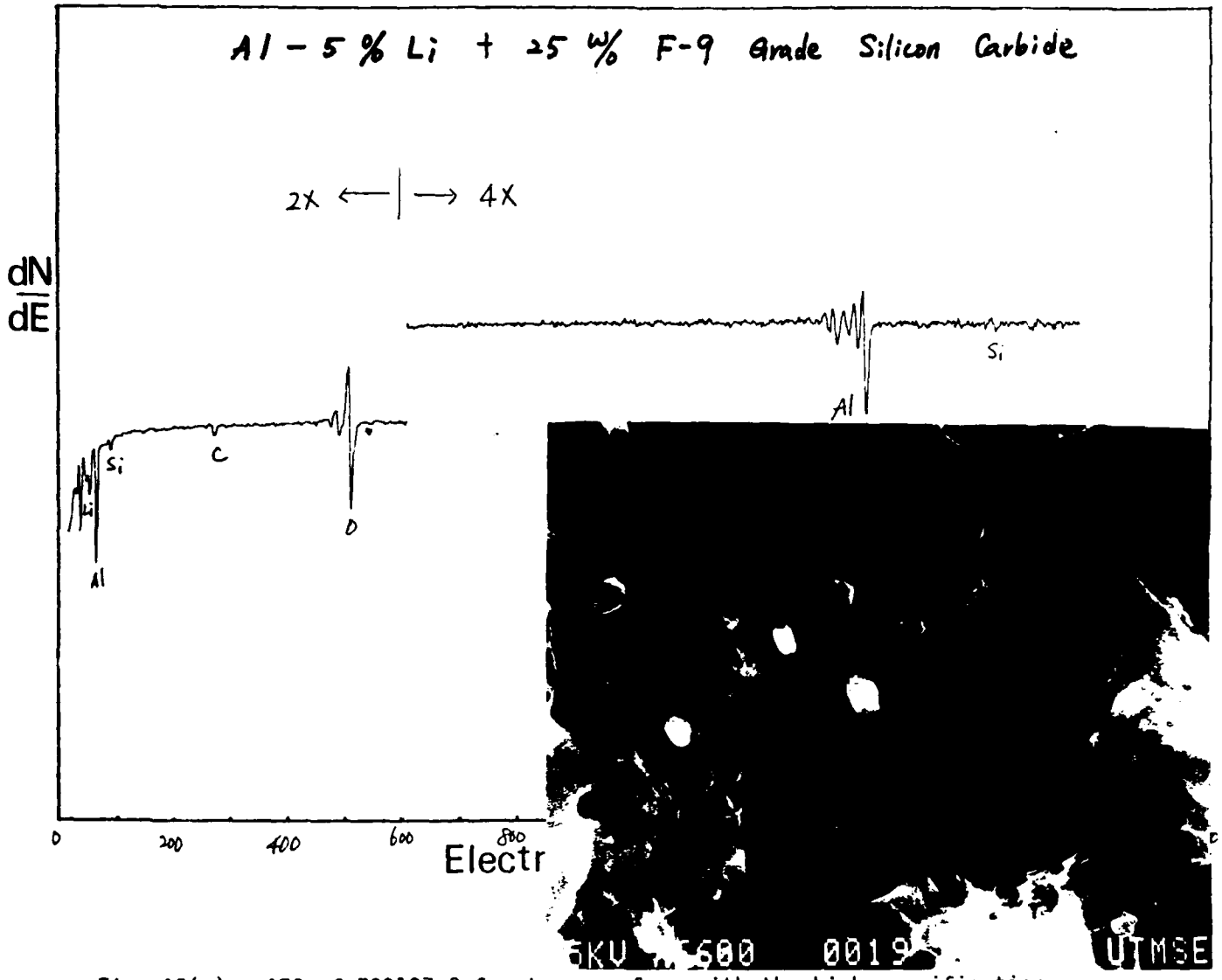

Fig. A5(a). AES of E0019Z-2 fracture surface with the high magnification SEM micrograph of the specimen.

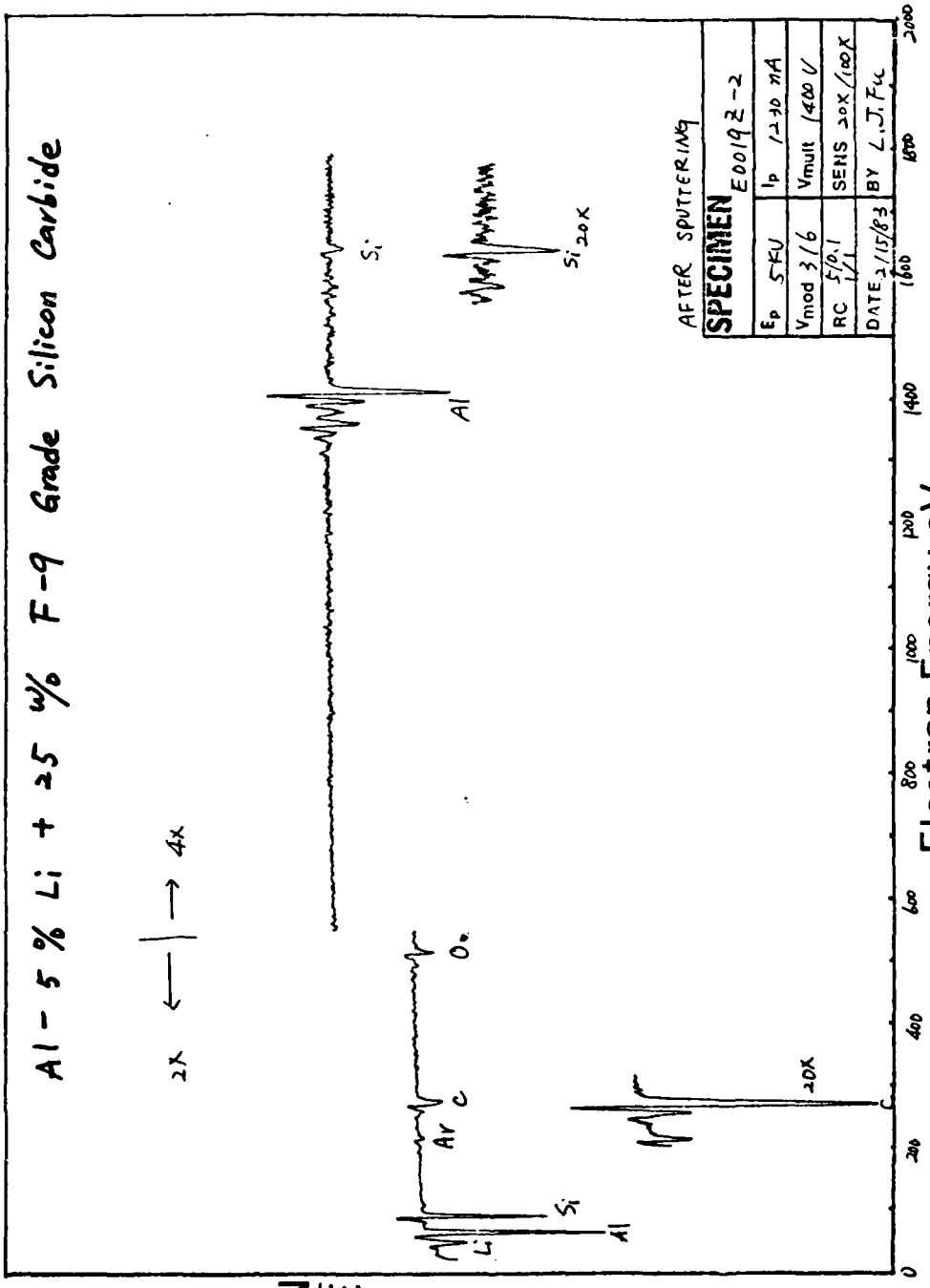

Fig. A5(b). AES of fracture surface of E00192-2 after inert ion sputtering (removed about 0.5 μm).

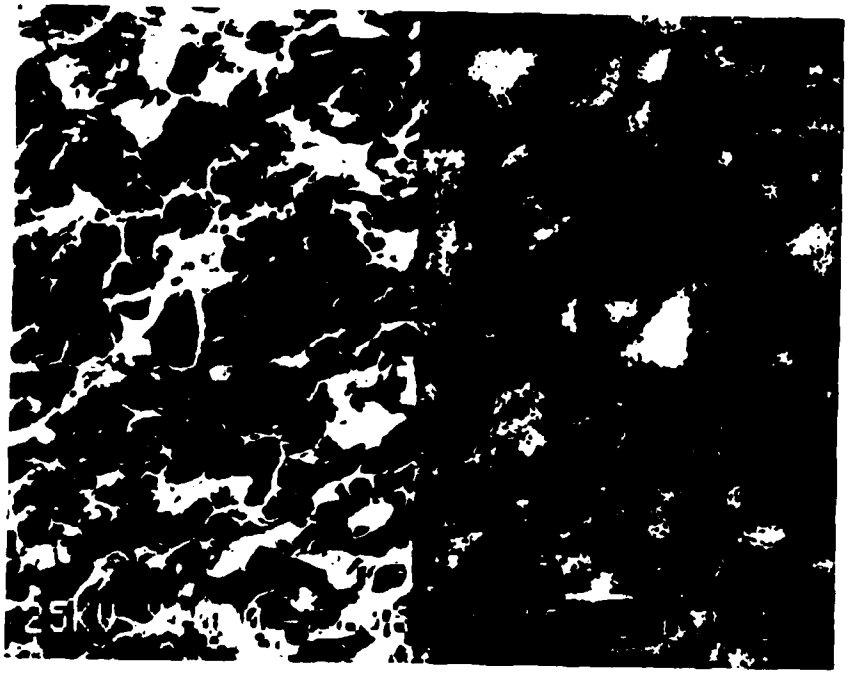

Fig. A6. SEM Si-mapping with related fracture surface of the 25 v/o Si-carbide powder/Al composite. The bright dots indicate the Si-carbide particles.

of quantitative analysis are listed in Table 2. The need to sputter a great depth to get the substantial SiC spectra gives strong support for high interface strength in the Si-carbide discontinuous fiber/Al composites.

Elemental maps of Si using EDS in the SEM differed from the Auger studies. The Si-carbide particles of fibers were observed in the elemental mapping even though the AES results indicate a layer of interface and matrix Al alloy over them. This is because many of the characteristic x-rays originate from a deeper volume in the bulk material.

A comparison of the 25 v/o Si-carbide powder/Al 6061 composite with C0116Z (Al 6061 + 30 w/o Si-carbide discontinuous fiber) follows. These two materials have the same metal matrix, and the C0116Z has larger SiC content by volume than that of the 25 v/o Si-carbide powder/Al composite. The quantitative AES results showed that the 25 v/o Si-carbide powder/Al composite had a larger Si concentration on the fracture surface. This indicates that more interface failure occurred in the Si-carbide powder/Al composite than in the Si-carbide discontinuous fiber/Al composite.

TEM Results

Extensive effort was spent on developing the thinning technique on the composites to form TEM samples. It was found that a 4 Kev accelerating ion beam voltage was optimum for thinning the aluminum metal matrix and the Si-carbide fibers or powders simultaneously.

A diffraction pattern taken from the jet-polished as received A6013Z specimen is identified as γ-Al_2O_3. Figure A7 shows the microstructure with the diffraction pattern of γ-Al_2O_3 along with a few diffraction

Table 2. Quantitative analysis of Auger spectra collected from fracture surfaces of Si-carbide fiber and Si-carbide powder in Al alloy matrices composites.

Material	Metal Matrix	SiC	Before Sputtering C_{Al} / C_{Si}	After Sputtering C_{Al} / C_{Si}	Theoretical Ratio for Known w/o or v/o of C_{Al} / C_{Si}
A6013Z	2024	22.45 w/o	10 : 1	3 : 1	3.45 : 1
C0115Z	6061	10 w/o	28 : 1	7 : 1	9 : 1
C0116Z	6061	30 w/o	7 : 1	3 : 1	2.33 : 1
D0026Z	7075	20 w/o	13 : 1	3 : 1	4 : 1
D0030Z-2	7075	5.7 w/o	88 : 1	11 : 1	16.45 : 1
E0019Z-2	Al-5% Li	25 w/o	4 : 1	4 : 1	3 : 1
SiC powder/Al	6061	25 v/o	5 : 1	5 : 1	3 : 1

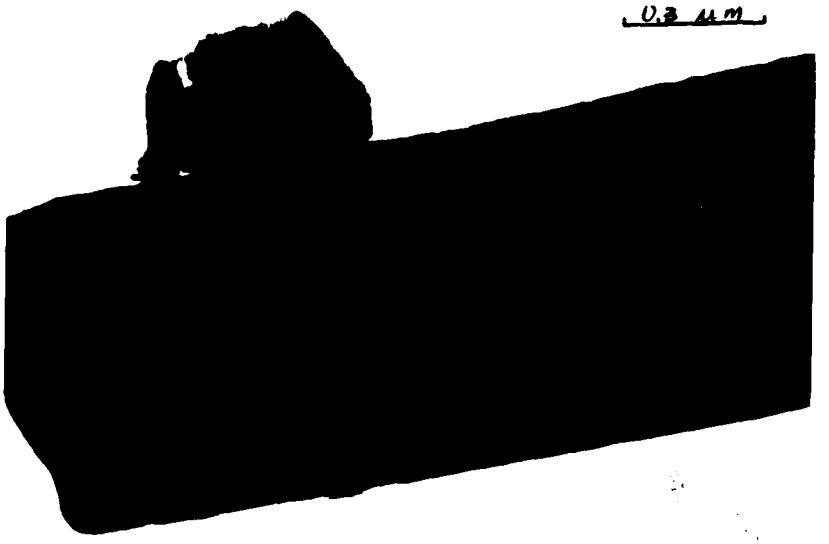

(a)

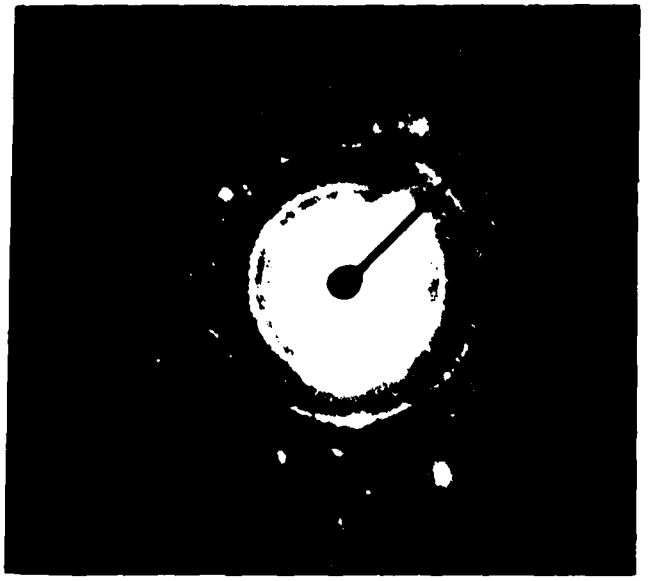

(b)

Fig. A7. The as-received A6013Z jet-polished specimen shows γ-Al_2O_3 is on the interface.

(a) Microstructure

(b) Diffraction pattern of γ-Al_2O_3 along with a few diffraction spots from the Al lattice.

spots from the Al lattice, and the indexing of γ-Al_2O_3 is listed in Table 5. γ-Al_2O_3 was also identified in both interfaces of as-received C0116Z and a heat treated A6013Z ion beam thinned longitudinal sections. Figures A8-a and A8-b are the TEM bright field and dark field micrographs of the interface of heat treated A6013Z longitudinal thinned section. The thickness of γ-Al_2O_3 phase is about 0.03 μm (only one variant of the γ-Al_2O_3 is seen in Fig. A8-b). The oxide phase was not uniformly present at every interface. A comparison of microstructures of heat treated and as-received transverse ion beam thinned A6013Z sections showed that there was no evidence of any significant reaction between Si-carbide fiber and Al matrix after annealing at 550°C in a diffusion-pumped rough vacuum (about $2x10^{-4}$ torr) conditions for 24 hours. A slight degradation was found by Kohara (6) at 600°C. The diffraction pattern taken from a transverse thinned section of A6013Z, shows the β-SiC (111) FCC reciprocal lattice plane in Fig. A9-b. The diffraction pattern of the aluminum adjacent to it shows a (001) FCC reciprocal lattice plane in Fig. A9-c, one of the Al projections found. γ-Al_2O_3 was not identified from this transverse thinned section. This may be due to the interface layer being too thin.

No interface phase was found in the Si-carbide powder/Al composite. Presumably, the interface region was too thin to observe in the limited number of samples prepared.

In order to compare the distributions of dislocations before and after tensile testing, the specimen C0116Z was chosen, because it has the most silicon-carbide content among the six types of as-received Si-

Table 3. The indexing procedure of γ-Al_2O_3 as well as a few diffraction spots from the Al lattice in Fig. A7(b).

r (cm)	Calculated d (Å)	I/I_0 (observed)	ASTM File d (Å)	Correlate Compound	I/I_1 (ASTM File)
0.8925	2.2565	30	2.28	γ-Al_2O_3	50
0.9950	2.0342		2.024	Al	47
1.0075	1.9989	90	1.977	γ-Al_2O_3	100
1.445	1.3937	90	1.395	γ-Al_2O_3	100
1.6575	1.2150		1.221	Al	24
1.7775	1.133	40	1.14	γ-Al_2O_3	20
2.0	1.0070		1.0124	Al	2
2.17	0.9281		0.9289	Al	8
2.275	0.8825	20	0.884	γ-Al_2O_3	10

(a)

(b)

Fig. A8. γ-Al_2O_3 was identified on the ion beam thinned longitudinal section of heat treated A6013Z section.

(a) Bright field microstructure.

(b) Dark field microstructure.

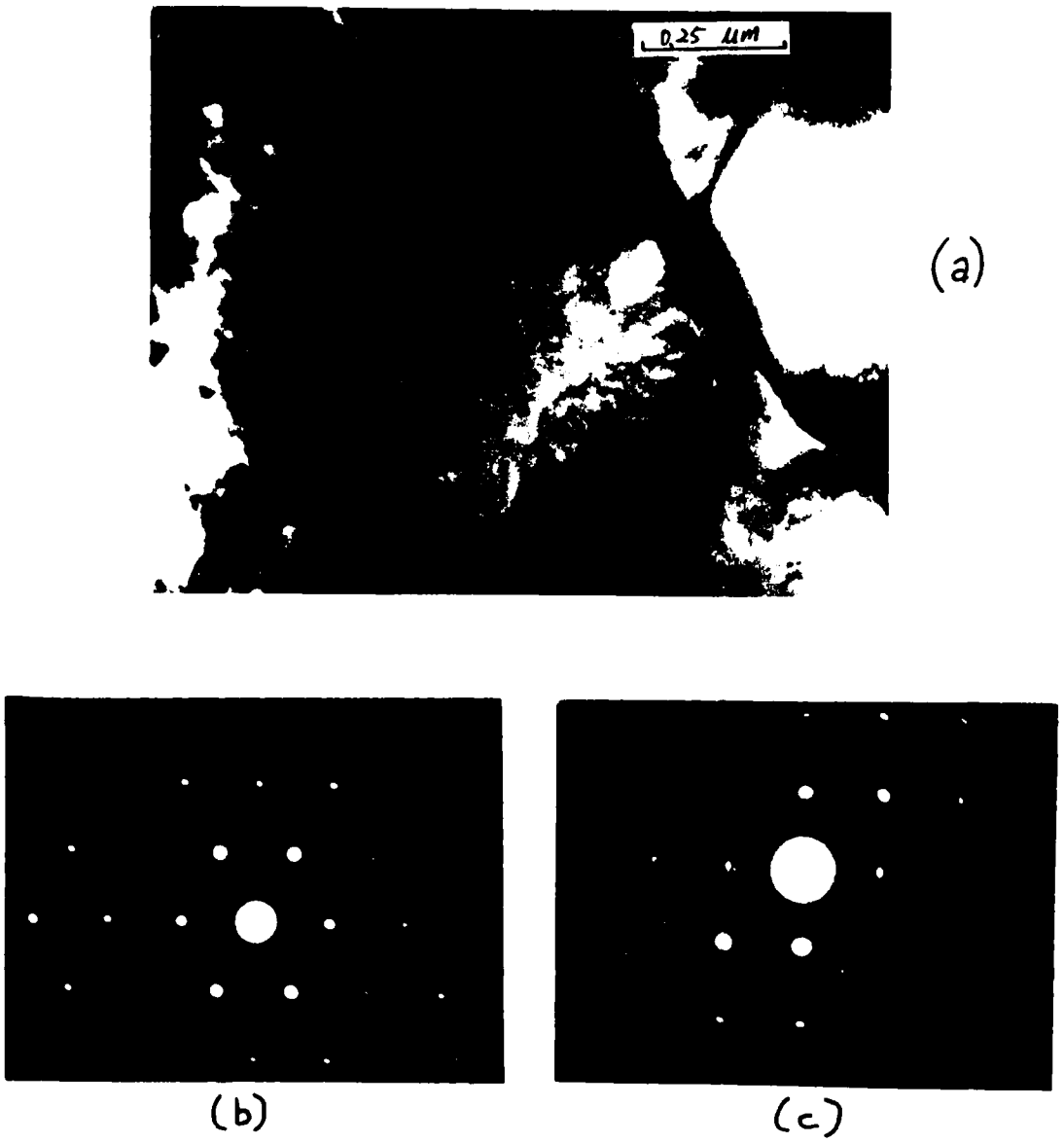

Fig. A9. Microstructure with diffraction pattern of ion beam thinned A6013Z transverse section.

(a) Microstructure of hexagonal cross-section shaped β-SiC fiber.

(b) (111) reciprocal lattice plane structure of the β-SiC fiber.

(c) The adjacent aluminum matrix showing the (001) reciprocal lattice plane.

carbide discontinuous fiber/Al composites. TEM microstructural analysis showed that there was not much difference between as-received and after tensile testing ion beam thinned C0116Z sections. A large dislocation density was found in the Al matrix in the vicinity of the silicon-carbide fibers in the as-received specimen (Figs. A10, A11). A similar dislocation density appeared in both the transverse and the longitudinal ion beam thinned A6013Z sections. The reason for the heavy dislocation density is postulated to be associated with deformation due to the large difference in thermal expansion coefficient and to that associated with the ion thinning process. There was no heavy dislocation density in the as-received and after tensile testing specimens of Si-carbide powder/Al composite (Fig. A12). This may be due to the small aspect ratio of the particulate material limiting the constraints. This also indicates that the ion thinning induced dislocation density does not dominate.

Conclusion

1. The more ductile the Al metal matrix, the less silicon-carbide fiber appears on the SEM micrograph of the fracture surface implying less interface fracture.
2. Silicon-carbide discontinuous fiber reinforced Al composites have strong interfaces. More SiC is observed on the fracture surface of silicon-carbide powder/Al composites.
3. Ion beam thinning at 4 Kev accelerating ion beam voltage allows for uniform thinning of the Si-carbide fibers or powders and Al matrix simultaneously for TEM analysis.

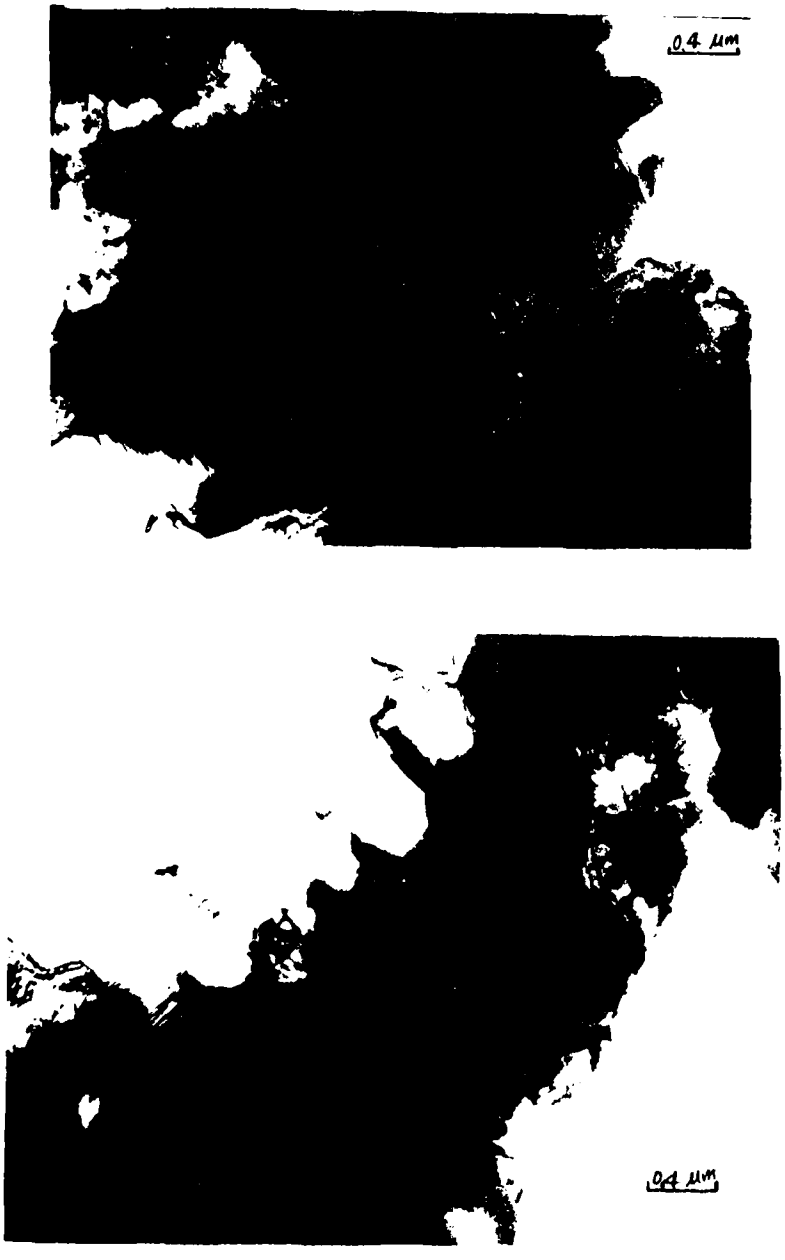

Fig. A10. Microstructures of as-received C0116Z specimen show the Al matrix in the vicinity of Si-carbide fiber has a large dislocation density.

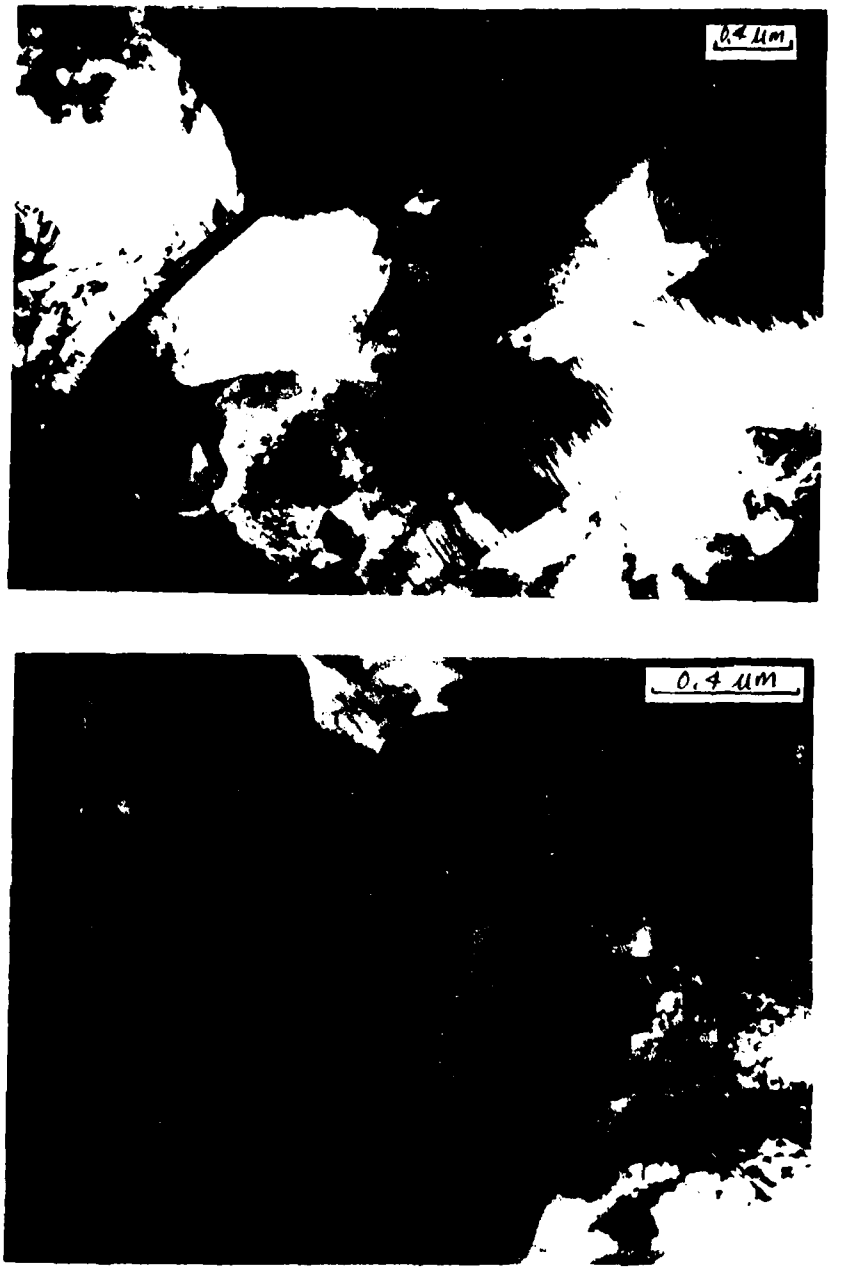

Fig. A11. Microstructures of C0116Z after tensile testing specimen. Both longitudinal and transverse direction fibers were in this type of specimen.

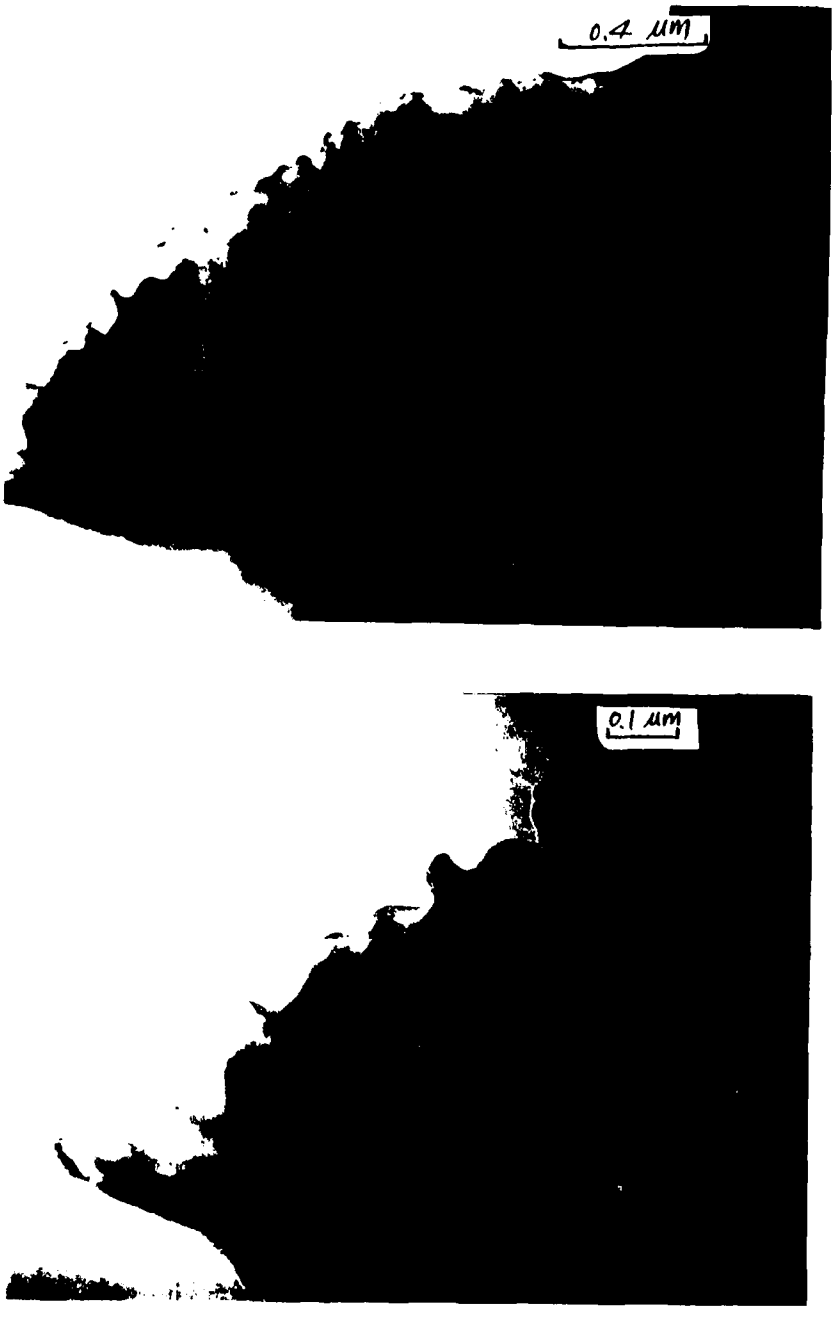

Fig. A12. Microstructures of ion beam thinned as-received Al 6061 + 25 v/o silicon-carbide powder specimen. Few dislocations occur around the SiC particles.

4. Very thin layers of γ-Al_2O_3 are in the interfaces of the discontinuous fiber SiC/Al composites, but not at all interfaces.

5. Interface failure does not play the dominant role in the reduction of ductility and fracture resistance.

Bibliography

1. A.P. Divecha, S.G. Fishman and S.D. Karmarker, "Silicon Carbide Reinforced Aluminum - A Formable Composite," Journal of Metals, September 1981, pp. 12-17.
2. A.P. Divecha and S.G. Fishman, "Mechanical Properties of Silicon Carbide Reinforced Aluminum," Mechanical Behavior of Materials, vol. 3, ICM, K.J. Miller and R.F. Smith, eds., Cambridge England, August 1979, pp. 351-361.
3. E.G. Wolff, "Hydrodynamic Alignment of Discontinuous Fibers in a Metal Matrix," Fiber Science and Technology, Elsevier Publishing Co., Essex, England, March 1969.
4. D. Finello, Doctoral Dissertation, The University of Texas at Austin, August 1982.
5. L.E. Davis, N.C. MacDonald, P.W. Palmberg, G.E. Riach and R.E. Weber, Handbook of Auger Electron Spectroscopy, 2nd ed., Physical Electronics Industries, Inc., 1976.
6. F.S. Lin, S.B. Chakraburtty and E.A. Starke, Jr., Met. Trans. 13A p. 461 (1982).
7. S. Kohara, "Compatibility of SiC Fibers with Aluminum," Composite Materials, K. Kawata and T. Akasaka, eds., Proc. Japan-US Conference Tokyo, 1981, pp. 224-227.

Appendix B

Quantitative Interface Strength Measurement

To define the causal relationship between thin film electronic states and cohesive strength, it will be necessary to quantify the fracture strength of the interfaces for comparison with other interface systems. To do this, three experimental systems are under study. Two of these systems measure load mechanically and one electromagnetically. The only difference in the two mechanical systems, Figs. B1 and B2, are the methods of system-thin film contact. In the first case, Fig. B1, a fast drying glue is used on a platen having approximate dimensions of the deposited thin film. In the second case, Fig. B2, a deposited magnetic film is used in conjunction with a permanent magnet to make contact. The glue has the disadvantage of possible contamination of the substrate and outgassing in the high vacuum AES chamber. The permanent magnet-magnetic film would produce a more uniform and geometrically definitive contact. The magnetic-mechanical system could use a flexible electromagnet instead of the permanent magnet. Both systems utilize a pure tensile interconnect link, possibly a light chain, and a load cell (e.g., 22.5 N). The substrate remains fixed in both systems.

A non-mechanical method of performing the peel test could be accomplished through the use of an electromagnetic set-up similar to the schematic of Fig. B3. Again, a magnetic film would be deposited on the composite thin film, but in this case a uniform magnetic field would be increased until interface separation occurred. The magnetic

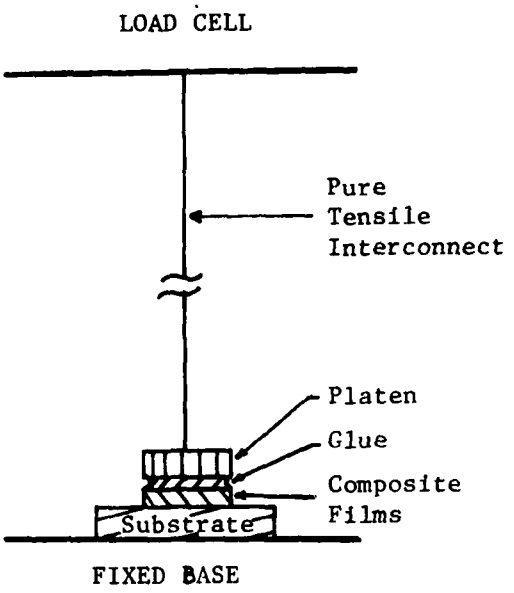

Fig. B1

Mechanical System

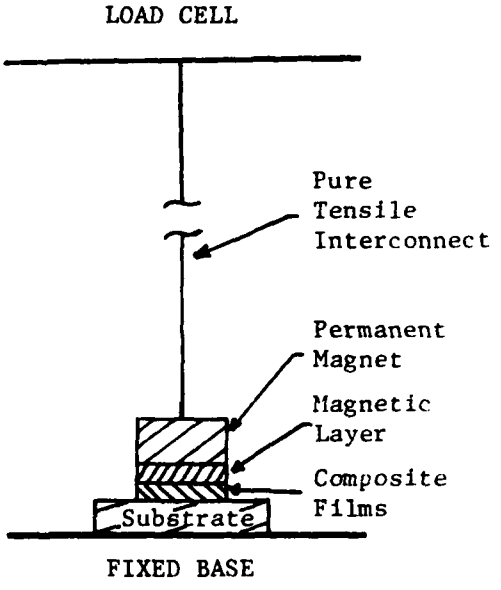

Fig. B2

Mechanical-Magnetic System

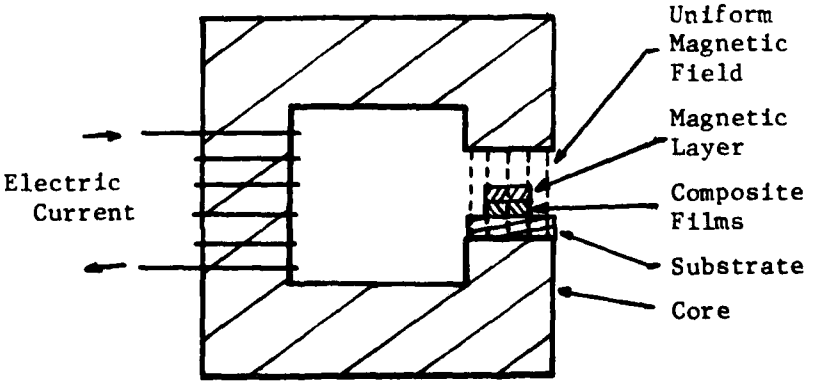

Fig. B3

Electromagnetic System

field strength could be correlated with load through the use of standards and known stress-strain relationships. The uniform field applies a uniform load on the thin film composite. In all cases the substrate remains fixed. All of these approaches are currently being explored.